instruments

MDPI

Article

Wide-Aperture Diffraction-Based Beam-Shaping Structures for Enhanced Directivity in Next-Generation High-Frequency Communication Systems

Vladislovas Čižas [1], Simonas Driukas [1], Andrius Masaitis [1,2], Kotryna Nacienė [1], Kasparas Stanaitis [1,2], Egidijus Šideika [3] and Linas Minkevičius [1,*]

[1] Department of Optoelectronics, Center for Physical Sciences and Technology, Saulėtekio Ave. 3, LT-10257 Vilnius, Lithuania
[2] Institute of Photonics and Nanotechnology, Vilnius University, Saulėtekio Ave. 9, LT-10222 Vilnius, Lithuania
[3] UAB 8Devices, Antakalnio St. 17, LT-10312 Vilnius, Lithuania; egidijus@8devices.com
* Correspondence: linas.minkevicius@ftmc.lt

Abstract

Sub-terahertz (sub-THz) frequencies are in the spotlight in the ongoing development of sixth-generation (6G) wireless communication systems, offering ultra-high data rates and low latency for rapidly emerging applications. However, employment of sub-THz frequencies introduces strict propagation challenges, including free-space path loss and atmospheric absorption, which limit coverage and reliability. To address these issues, highly directional links are required. The conventional beam-shaping solutions such as refractive lenses and parabolic mirrors are bulky, heavy, and costly, making them less attractive for compact systems. Diffractive optical elements (DOEs) offer a promising alternative by enabling precise wavefront control through phase modulation, resulting in thin, lightweight components with high focusing efficiency. Employing the fused deposition modelling (FDM) using high-impact polystyrene (HIPS) allows cost-effective fabrication of DOEs with minimal material waste and high diffraction efficiency. This work investigates the beam-shaping performance of the FDM-printed structures comparing DOEs and spherical refraction-based structures, wherein both are aiming for application in sub-THz communication systems. DOEs exhibit clear advantages over classically employed solutions.

Keywords: diffractive optical elements; beam shaping; sub-terahertz band; high-impact polystyrene; high-frequency communication; fused deposition modelling

Academic Editor: Antonio Ereditato

Received: 8 January 2026
Revised: 30 January 2026
Accepted: 1 February 2026
Published: 4 February 2026

1. Introduction

The sub-terahertz (sub-THz) frequency range is considered to be a key enabler for next-generation wireless communication systems such as 6G [1–3]. High carrier frequencies, typically employing the 60–300 GHz range, provide very wide bandwidths, allowing high data throughput, which is essential for the ever-growing number of consumers and devices, as well as enabling massive Internet of Things (IoT) platforms [4,5]. For example, the unlicensed 60 GHz band offers several gigahertz of spectrum, enabling multi-gigabit wireless links in standards like [6,7]. However, operating at such high frequencies introduces free-space path losses and atmospheric absorption, which significantly reduce signal strength and coverage [8,9]. Free-space path loss increases with frequency—at 60 GHz, it is approximately 20–30 dB higher compared to currently most employed microwave bands (e.g., 2–5 GHz). In addition, the 60 GHz band experiences atmospheric absorption

on the order of 10–15 dB per kilometre [10,11]. To mitigate these losses, highly directional free-space transmission links between the emitter and receiver parts of the network are essential. To guarantee high-intensity carrier beam propagation, it is important to enhance the emitter directivity properties [12,13].

One of the most effective ways to improve directivity and extend the effective propagation distance is optical beam collimation, allowing us to maintain concentrated irradiance path in free space. Traditional solutions such as refractive lenses and parabolic mirrors used for beam focusing are often heavy, bulky, and expensive [14,15]. Thick lenses may also add extra material-dependent absorption losses and in combination with their size make integration into compact systems difficult and less efficient. Diffractive optical elements (DOEs) offer a promising alternative for beam control [14,16–18]. These components use wavefront engineering to control phase via constructive interference, enabling focusing, beam steering, and wavefront tailoring with millimetre-scale thickness and low-mass elements [19–22]. They also enable the achievement of a lower F-number, ensuring close focusing with a wide aperture, required for integration into compact devices. Recent advances in additive manufacturing, particularly fused deposition modelling (FDM) using high-impact polystyrene thermoplastic material (HIPS) [23], have demonstrated cost-effective production of DOEs with minimal material waste. It has been shown that 3D-printed DOEs can provide high focusing efficiency and compact designs, making them suitable for complex sub-THz communication systems [21,24–26]. Printable diffractive optics can be a great beam-shaping alternative, applicable in sub-THz communication field. It allows us to maintain or even increase the efficiency of optical systems, while decreasing their physical parameters, weight and production cost. These characteristics are particularly relevant for scenarios requiring multiple highly directive links deployed in close proximity, such as dense urban access points and indoor network infrastructures. This allows for integration opportunities into small, easily integrable communication devices, which is relevant for production of densely packed 5G/6G stations in urban areas [12].

In this work, we focus on the design and modelling of FDM-printed diffractive elements for sub-THz communication systems. We analyse the potential use of Fresnel lenses and their variations to improve link directivity, reduce propagation losses, and enable scalable integration into next-generation wireless networks. Finally, experimental results are also provided, demonstrating link directivity improvements over an uncollimated beam, as well as a comparison to the conventional spherical lens.

2. Materials and Methods

The present investigation focuses on the development of DOEs designed to collimate electromagnetic radiation emitted by a commercial 60 GHz source. Beam-shaping is achieved using a diffraction-based element, which is configured employing a non-paraxial phase-surface design equation, expressed as

$$\varphi(x,y) = -k\left(\sqrt{f^2+(x-x_0)^2+(y-y_0)^2} - \sqrt{f^2+x_0^2+y_0^2}\right). \quad (1)$$

Here, k is a wavenumber, f is the focal length, x and y are phase-surface coordinates, and x_0 and y_0 are the focal point coordinates. The required phase-shift for the calculated profile of the structure was achieved by varying the thickness of the structure at each point of the phase surface. HIPS was selected for the fabrication due to its compatibility with a simple and cost-efficient 3D printing method, as well as its refractive index of $n = 1.53$ [27], allowing us to achieve 2π phase modulation by increasing the thickness of the diffractive element by 7 mm. Designs have been fabricated employing a Creality K1 (Creality 3D Technology Co., Ltd., Shenzhen, China) extrusion 3D printer. Despite being compatible

with the smaller ones, a printer nozzle with a diameter of 0.4 mm was chosen intentionally to reduce the fabrication time and in turn the possibility of printing errors. The selected nozzle diameter is considered small enough, since it is an order of magnitude smaller than the wavelength of interest, making the surface roughness effectively invisible to sub-THz radiation. A vertical resolution of 0.1 mm was set to ensure good quality in every layer. A printing infill of 100% was used to ensure a continuous optical path within the lens material, which is crucial for lens performance. The printing of one component takes ≈6 h. The elements were designed in the shape of a 12 cm × 12 cm square with a supporting frame of 1 cm width. The elements were printed on an HIPS base of 2 mm thickness. Additional holes were drilled for the mounting of the lens, as shown in Figure 1b.

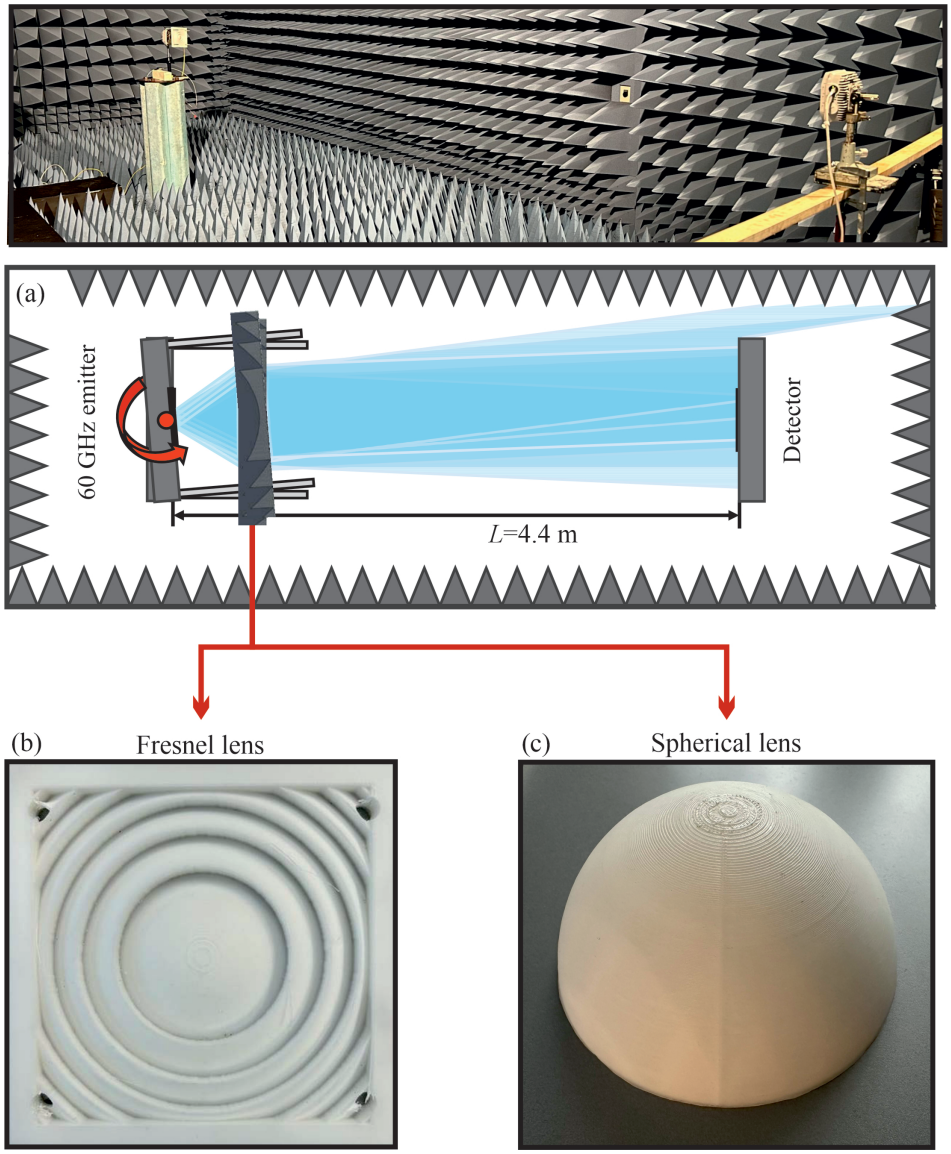

Figure 1. (**a**) Schematic representation of the experimental setup for angular characterisation of the structures. The measurement was conducted in an anechoic chamber. The emitter and the designed element were rigidly mounted, and the assembly was positioned on an angle-controlled tripod. At a distance of 4.4 m, a detector—the same chip, but without any beam-shaping solution—was placed. Angular intensity dependency was achieved by rotating the source coupled with the element. The inset above reveals a photo of the anechoic chamber during the characterisation. (**b**) A photo of one of the fabricated Fresnel type lenses, with a structure thickness of 7 mm. (**c**) A photo of the spherical lens, featuring an identical focal distance, with a structure thickness of 74 mm.

The commercial Peraso PRM2141X mmWave Module (Peraso Technologies Inc., San Jose, CA, USA) was employed as the emitter and detector for the characterisation of the fabricated lenses. The detector/emitter operates in the millimetre-wave V-band and is equipped with a 16-element phased-array antenna supporting enhanced electronic beam-shaping. The array provides a maximum gain of 16.1 dBi and a maximum EIRP of 38 dBm. The antenna exhibits a -10 dB beamwidth in the range of 79–115°, which is channel-dependent and results in less than -3 dB gain degradation under small beam-steering angles. A frequency of 60 GHz was initially chosen, although the emitter is designed to operate across the 57–71 GHz range covering 13 channels according to the 802.11 ad [7]. Such capabilities of the emitter facilitate future studies related to the compatibility of the proposed and existing solutions across the whole range of operation. The same module, but without any beam-shaping solution, was used as a detector in the setup.

The fabricated elements were characterised by measuring the spatial signal distribution (intensity dependency on the angle). This was performed in an anechoic chamber environment to avoid any external noise and reflection from different surfaces. The chamber dimensions are 8.4 m × 4.6 m × 3.7 m. Conforming to the IEC EN 61000-4-3 standard for electromagnetic emission measurement, the anechoic chamber provides a perfect environment for the research of next-generation communication systems and their components [28]. Fabricated lenses were rigidly mounted on the 60 GHz emitter at the focal distance of the structure (the focal distance was checked by measuring the same setup and adjusting the distance between the source and the sample). The system was placed on an angle-controlling tripod, covering 180 degrees of the horizontal plane. The detector was positioned at a 0-degree angle at the same height and kept at a constant position. The distance between the source and the detector was kept constant at $L = 4.4$ m. By rotating the emitter–lens system, a full 180-degree beam profile was recorded. Rotation in the vertical plane was not performed due to lens and emitter antenna array symmetry. The experimental setup is displayed in Figure 1a.

3. Results

In order to ensure the correctness of the design, prior to the fabrication, the beam-shaping abilities of the generated structures were theoretically checked. This was done by employing the FDTD method provided by the CST Studio Suite 2026 (Dassault Systemes Simulia Corp., Johnston, RI, USA) software. Figure 2a presents simulations of the beam-shaping element in which the refractive index of the material is varied. During these simulations, the design of the structure was adjusted to account for the changed refraction index. The refractive index was varied over the range from 1.3 to 1.7 to account for the limited accuracy of the TDS-based measurement method at the 60 GHz operating frequency, as the TDS characterisation system specifies reliable performance only down to 100 GHz. The simulations reveal that beam-shaping structure fabrication is possible in a considerably wide range of the refractive index; however, a significant impact on the electric field strength at the focal point exists at low refraction indexes. A change in electric field strength by approximately 12% has been observed for a refraction index change of $\Delta n = 0.2$. It is additionally revealed in Figure 2b that an increase in the lens cross-sectional width (the non-optical, volumetric portion used for mechanical support rather than focusing) shifts the focal point slightly toward the lens, but the displacement is negligible and does not influence the radiation intensity.

The detailed modelling analysis led to a selection of optimal Fresnel lens parameters for collimating the emitter beam. A lens diameter of 12 cm and a mounting-base thickness of 2 mm were chosen, resulting in an effective average lens thickness of 9 mm. Full width at half maximum (FWHM) and depth of focus (DOF) are considered the main beam-shaping

efficiency-characterising parameters at the particular stage of the research. As revealed at Figure 3, $FWHM = 4.3$ mm and $DOF = 13.3$ mm have been observed. The Fresnel lens design yielded a focal length of 54 mm, corresponding to an F-number of $F\# = 0.45$. For comparison with the non-paraxial diffractive design, a conventional refraction-based spherical lens was also designed and fabricated. A similar focal length of 50 mm was selected for this lens; however, the resulting F-number was higher, at $F\# = 0.74$.

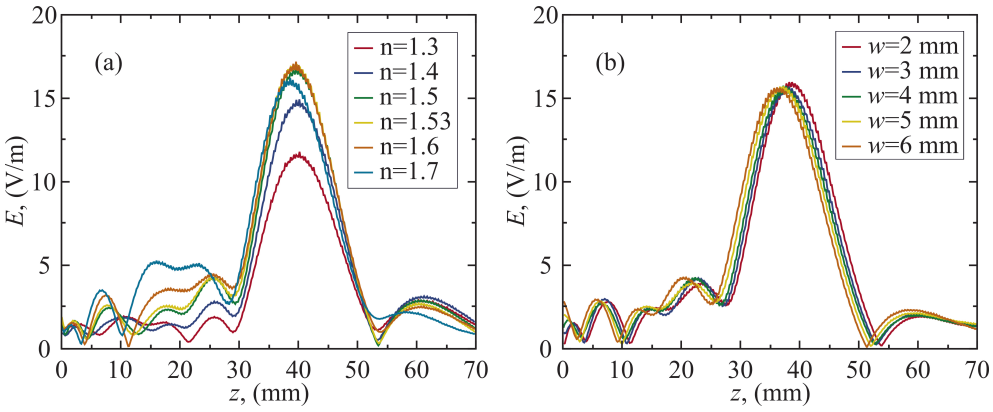

Figure 2. Electric field strength intensity profiles along the optical axis for structures of different refractive index (**a**) and base layer thickness (**b**). The refraction index sweep reveals the beam-shaping abilities of the structures, fabricated from different materials of different refraction indexes. A decrease in efficiency is observed with a decrease in the refraction index. Base layer thickness is shown to have an insignificant effect on the beam-shaping abilities of the structure due to low absorption of the frequency range of interest in the material.

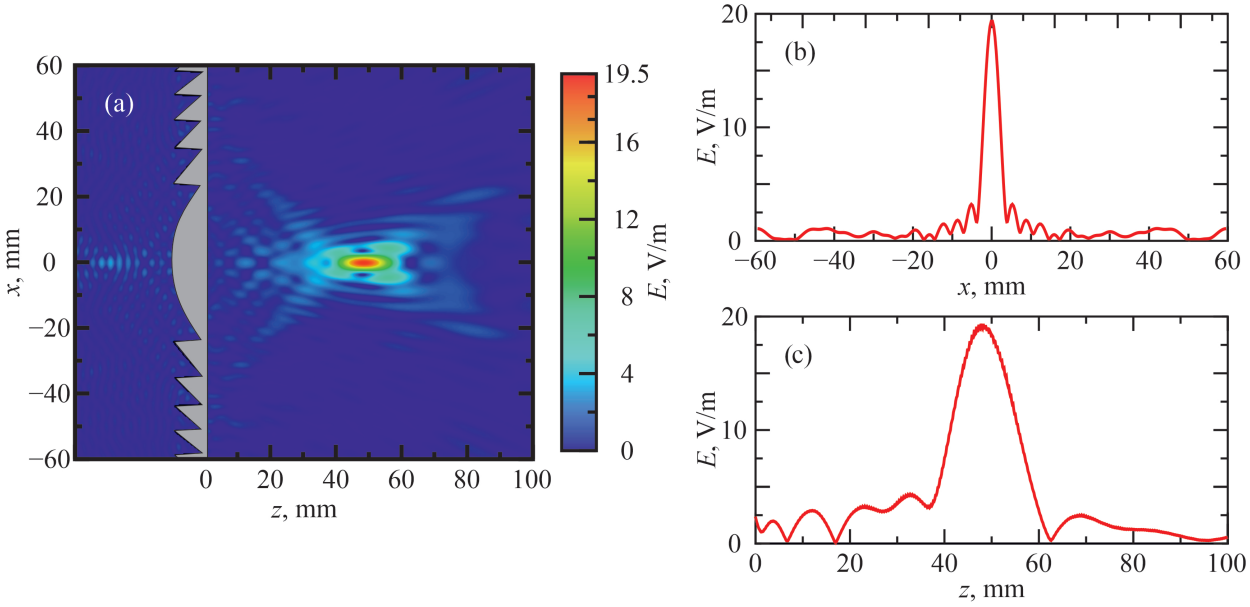

Figure 3. Electric field strength distribution of the lens, selected for fabrication (diameter 12 cm, designed focal distance 50 mm). Distributions are revealed for the x-z plane (**a**) and for the main lines of interest: perpendicular to the optical axis at focal point (**b**) and along the optical axis (**c**). Full width at half maximum (FWHM) of 4.3 mm and depth of focus (DOF) of 13.3 mm have been observed.

The main experimental results consist of detailed emitter beam directivity measurements incorporating conventional spherical lens and a wide-aperture Fresnel lens. The acquired angular beam dependencies for the bare emitter or the emitter system enhanced with either a spherical or Fresnel lens are presented in Figure 4. The performance of the beam-shaping solution is compared in terms of both the spatial profile of the colli-

mated beam and its intensity at the target direction, e.g., 0° intensity. Considering the spatial profile, both the spherical and Fresnel lenses exhibit a significant reduction in the FWHM compared to the directivity of the bare emitter (the FWHM of the bare emitter was found to be $FWHM_{\text{bare}} \approx 37.8°$). However, the difference in collimated beamwidth between the two lenses was found to be considerably small; the spherical lens resulted in an FWHM of $FWHM_{\text{Spherical}} \approx 3.23°$ compared to $FWHM_{\text{Fresnel}} \approx 3.19°$ for the Fresnel lens. This indicates that the phase-domain beam-shaping mechanism in the fabricated Fresnel lens achieves an efficiency comparable to that of conventional refraction-based lenses. The advantage, due to the lower absorption of the material of the proposed diffractive beam-shaping solution, arises when comparing the target intensity of the lenses. In the case of Fresnel lens, a distinct enhancement is observed, compared to the classical spherical lens. The measured beam intensities between the two lenses differ by more than one order: −0.64 μW for the spherical element and 8 μW for the Fresnel lens.

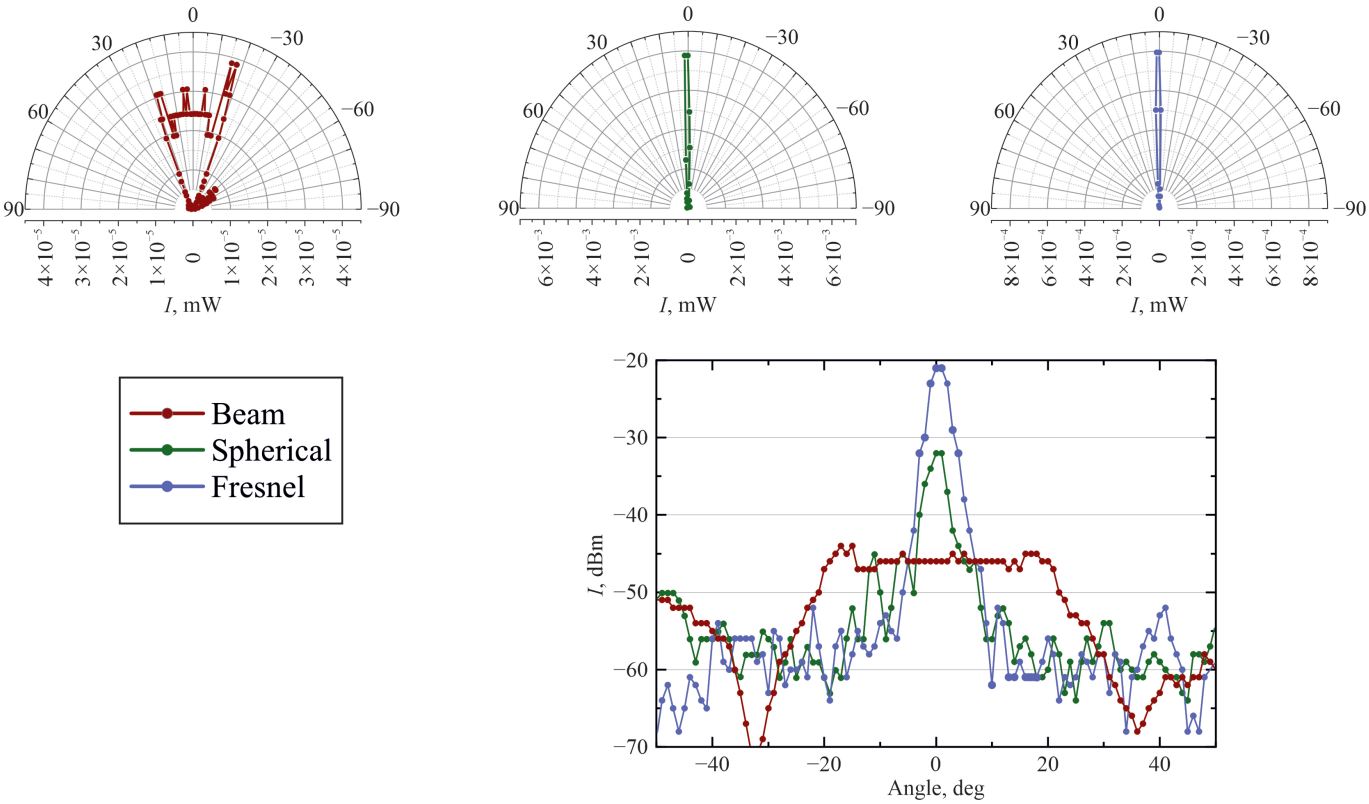

Figure 4. Angular power distribution (in dBm) for the bare emitter or the emitter system, enhanced with spherical or Fresnel beam-shaping solution. The insets above reveal the same distribution on the mW scale and in the polar coordinate system. Note a similar increase in beam-shaping directivity efficiency, arising by enhancing the system with a beam-shaping solution (an FWHM decrease by 10 times is observed). Also note a significantly larger 0° intensity for the system, enhanced with the Fresnel beam-shaping structure compared to the spherical beam-shaping structure.

The pronounced increase in beam intensity can be attributed to two primary factors. The first is related to the absorption of the emitted signal within the lens material. The effective thicknesses of the Fresnel and spherical lenses were 7 mm and 74 mm respectively. Considering the absorption coefficient of the HIPS polymer at 60 GHz to be 10 m^{-1} [29], the corresponding absorption losses were estimated at 6.8% and 32.3%. Although these values indicate a notable contribution to the overall intensity attenuation, lens absorption losses alone are insufficient to explain the experimentally observed differences between the two lenses. The second contributing factor concerns the numerical aperture (NA) of the collimating lens. When the emitter is positioned close to the lens, a high NA is essential

to effectively capture the broad radial emission of the active 4 × 4 phased-array antenna. The related *F*# values for spherical and Fresnel lenses are 0.74 and 0.45; thus, in the latter case, a more significant part of the emitter beam is captured. This may be the defining factor of the observed experimental result and the differences in 0° intensity. Overall, a clear advantage of the diffraction-based lens can be seen compared to the conventional, spherical lens design.

4. Discussion

The presented research is expected to significantly contribute to the extensively emerging new generation communication technologies including but not limited to the 60 GHz-based network. Until now, in newly appearing commercially available products, employment of diffractive beam-shaping elements is found as vague or non-existent. The proposed research reveals promising possibilities for the practical implementation of these components, leading to 12.5 times more efficient beam-shaping (0° intensity wise), which in turn lays the foundation for the enhanced implementation of 6G+ communication technology in real-life applications.

The results indicate that the proposed approach maintains comparable beam-shaping efficiency while achieving a higher target intensity at 0°, thereby outperforming classical refraction-based beam-shaping solutions. While similar beam spread is maintained, the Fresnel structure shows a pronounced increase in the on-axis (0°) intensity exceeding one order of magnitude. This approach provides significant fabrication material savings as a result of the substantially decreased structural volume, thereby reducing the mass of the final solution. Finally, the use of diffraction-based beam-shaping solutions offers an additional advantage: since the element design is defined in the phase plane, it can be readily adapted to generate not only focused Gaussian beams but also other beam types, such as Bessel, Airy, and related structured beams. Although the present study focuses on a single proof-of-concept structure operating at a representative frequency, the underlying design methodology is not limited to these parameters. The approach can be straightforwardly extended to different frequencies, focal distances, and beam-shaping requirements, forming a basis for future systematic investigations. This provides additional flexibility, leading to better adaptation and efficiency in particular tasks.

In summary, the investigated diffraction-based lens revealed highly efficient beam collimation, surpassing the traditional refractive lens and offering promising opportunities for employment in close-range high-speed/high-volume data transfer systems. Further development of such systems is considered crucial to further enhance currently emerging wireless communication networks in densely populated environments and to address the rapidly increasing number of IoT solutions oriented toward smart city and smart environment applications.

Author Contributions: Conceptualisation, L.M. and E.Š.; methodology, V.Č.; software, K.S.; validation, K.S. and S.D.; formal analysis, K.S.; investigation, K.S. and K.N.; resources, K.N.; data curation, K.N.; writing—original draft preparation, A.M., K.N. and S.D.; writing—review and editing, V.Č.; visualisation, A.M. and V.Č.; supervision, L.M.; project administration, L.M.; funding acquisition, L.M. All authors have read and agreed to the published version of the manuscript.

Funding: This research received no external funding.

Data Availability Statement: Data underlying the results presented in this paper may be obtained from the authors upon reasonable request.

Acknowledgments: The authors would like to express their sincere gratitude to Sergej Orlov for the valuable, illuminating, and encouraging discussions related to diffractive optics and Paulius Ragulis for the help with experimental measurements in the anechoic chamber.

Conflicts of Interest: Author Egidijus Šideika was employed by the company "UAB 8Devices". The authors declare there is no conflict of interests.

Abbreviations

The following abbreviations are used in this manuscript:

DOE	Diffractive Optical Element
DOF	Depth of Focus
FDM	Fused Deposition Modelling
FDTD	Finite-Difference Time-Domain
FWHM	Full Width at Half Maximum
GHz	Gigahertz
HIPS	High-Impact Polystyrene
NA	Numerical Aperture
TDS	Time-Domain Spectroscopy
THz	Terahertz

References

1. Yeh, C.; Do Jo, G.; Ko, Y.J.; Chung, H.K. Perspectives on 6G wireless communications. *ICT Express* **2023**, *9*, 82–91. [CrossRef]
2. Jiang, W.; Zhou, Q.; He, J.; Habibi, M.A.; Melnyk, S.; El-Absi, M.; Han, B.; Renzo, M.D.; Schotten, H.D.; Luo, F.L.; et al. Terahertz Communications and Sensing for 6G and Beyond: A Comprehensive Review. *IEEE Commun. Surv. Tutor.* **2024**, *26*, 2326–2381. [CrossRef]
3. Atzeni, I.; Tejerina, G.R.d.L.; Berkvens, R.; Chen, H.; Conrat, J.M.; Guzman, M.F.D.; Desset, C.; Dörpinghaus, M.; Farhadi, H.; Fettweis, G.; et al. Sub-THz Communications: Perspective and Results From the Hexa-X-II Project. *IEEE Open J. Commun. Soc.* **2025**, *6*, 7495–7540. [CrossRef]
4. Kleine-Ostmann, T.; Nagatsuma, T. A review on terahertz communications research. *J. Infrared Millim. Terahertz Waves* **2011**, *32*, 143–171. [CrossRef]
5. Vettikalladi, H.; Sethi, W.T.; Ko, W. Sub-terahertz (THz) antenna for Internet of Things and 6G Communication. *Frequenz* **2021**, *76*, 177–184. [CrossRef]
6. Niu, Y.; Li, Y.; Jin, D.; Su, L.; Vasilakos, A.V. A survey of millimeter wave communications (mmWave) for 5G: Opportunities and challenges. *Wirel. Netw.* **2015**, *21*, 2657–2676. [CrossRef]
7. *IEEE Std. 802.11ad-2012*; IEEE Standard for Information Technology—Telecommunications and Information Exchange Between Systems—Local and Metropolitan Area Networks— Specific Requirements—Part 11: Wireless LAN Medium Access Control (MAC) and Physical Layer (PHY) Specifications, Amendment 3: Enhancements for Very High Throughput in the 60 GHz Band (IEEE 802.11ad-2012). IEEE Standards Association: Piscataway, NJ, USA, 2012. Available online: https://standards.ieee.org/ieee/802.11ad/4527/ (accessed on 7 January 2026).
8. Slocum, D.M.; Slingerland, E.J.; Giles, R.H.; Goyette, T.M. Atmospheric absorption of terahertz radiation and water vapor continuum effects. *J. Quant. Spectrosc. Radiat. Transf.* **2013**, *127*, 49–63. [CrossRef]
9. Taleb, F.; Alfaro-Gomez, M.; Al-Dabbagh, M.D.; Ornik, J.; Viana, J.; Jäckel, A.; Mach, C.; Helminiak, J.; Kleine-Ostman, T.; Kürner, T.; et al. Propagation of THz radiation in air over a broad range of atmospheric temperature and humidity conditions. *Sci. Rep.* **2023**, *13*, 20782. [CrossRef]
10. Rappaport, T.S.; Sun, S.; Mayzus, R.; Zhao, H.; Azar, Y.; Wang, K.; Wong, G.N.; Schulz, J.K.; Samimi, M.; Gutierrez, F. Millimeter Wave Mobile Communications for 5G Cellular: It Will Work! *IEEE Access* **2013**, *1*, 335–349. [CrossRef]
11. Smulders, P. Exploiting the 60 GHz band for local wireless multimedia access: Prospects and future directions. *IEEE Commun. Mag.* **2002**, *40*, 140–147. [CrossRef]
12. Ahamed, M.M.; Faruque, S. 5G network coverage planning and analysis of the deployment challenges. *Sensors* **2021**, *21*, 6608. [CrossRef] [PubMed]
13. Singh, A.; Petrov, V.; Sen, P.; Jornet, J.M. Near-Field Terahertz Communications for 6G and Beyond: From concepts to realizations. *IEEE Signal Process. Mag.* **2025**, *42*, 106–125. [CrossRef]
14. Siemion, A. Terahertz Diffractive Optics—Smart Control over Radiation. *J. Infrared Millim. Terahertz Waves* **2019**, *40*, 477–499. [CrossRef]
15. Margheri, G.; Del Rosso, T. Tunable Device for Long Focusing in the Sub-THz Frequency Range Based on Fresnel Mirrors. *Micromachines* **2024**, *15*, 715. [CrossRef]

16. Wentworth, F.; Wiltse, J.; Sobel, F. Quasi-optical surface waveguide and other components for the 100-to 300-Gc region. *IRE Trans. Microw. Theory Tech.* **1961**, *9*, 512–518. [CrossRef]
17. Siemion, A. The Magic of Optics—An Overview of Recent Advanced Terahertz Diffractive Optical Elements. *Sensors* **2020**, *21*, 100. [CrossRef]
18. Komorowski, P.; Kaluza, M.; Surma, M.; Siemion, A. 3D printed diffractive lenses operating at 1 THz. *Lith. J. Phys.* **2023**, *63*, 122. [CrossRef]
19. Wiltse, J.C. Diffraction optics for terahertz waves. In Proceedings of the Terahertz for Military and Security Applications II, Orlando, FL, USA, 12–16 April 2004; SPIE: St Bellingham, WA, USA, 2004; Volume 5411, pp. 127–135. [CrossRef]
20. Ivaškevičiūtė-Povilauskienė, R.; Kizevičius, P.; Nacius, E.; Jokubauskis, D.; Ikamas, K.; Lisauskas, A.; Alexeeva, N.; Matulaitienė, I.; Jukna, V.; Orlov, S.; et al. Terahertz structured light: Nonparaxial Airy imaging using silicon diffractive optics. *Light Sci. Appl.* **2022**, *11*, 326. [CrossRef]
21. Kaluza, M.; Komorowski, P.; Zagrajek, P.; Siemion, A. Terahertz focusing blazed diffractive optical elements for frequency demultiplexing. *Adv. Opt. Technol.* **2023**, *12*, 1310578. [CrossRef]
22. Orlov, S.; Ivaškevičiūtė-Povilauskienė, R.; Mundrys, K.; Kizevičius, P.; Nacius, E.; Jokubauskis, D.; Ikamas, K.; Lisauskas, A.; Minkevičius, L.; Valušis, G. Light Engineering and Silicon Diffractive Optics Assisted Nonparaxial Terahertz Imaging. *Laser Photonics Rev.* **2024**, *18*, 2301197. [CrossRef]
23. Stanaitis, K.; Čižas, V.; Bielevičiūtė, A.; Grigelionis, I.; Minkevičius, L. High-Impact Polystyrene Structured Light Components for Terahertz Imaging Applications. *Sensors* **2024**, *25*, 131. [CrossRef] [PubMed]
24. Squires, A.D.; Constable, E.; Lewis, R.A. 3D Printed Terahertz Diffraction Gratings And Lenses. *J. Infrared Millim. Terahertz Waves* **2014**, *36*, 72–80. [CrossRef]
25. Furlan, W.D.; Ferrando, V.; Monsoriu, J.A.; Zagrajek, P.; Czerwińska, E.; Szustakowski, M. 3D printed diffractive terahertz lenses. *Opt. Lett.* **2016**, *41*, 1748. [CrossRef] [PubMed]
26. Komorowski, P.; Siemion, A.; Walczakowski, M.; Zagrajek, P. The Role of the Directivity of Various THz Detectors in Multiplexing Systems. *Appl. Sci.* **2022**, *12*, 3545. [CrossRef]
27. Stanaitis, K.; Redeckas, K.; Bielevičiūtė, A.; Bernatonis, M.; Jokubauskis, D.; Čizas, V.; Minkevičius, L. Study of the low-cost HIPS and paraffin-based terahertz optical components. *Lith. J. Phys.* **2023**, *63*, 233–240. [CrossRef]
28. *IEC 61000-4-3:2020*; Electromagnetic Compatibility (EMC)—Part 4-3: Testing and Measurement Techniques—Radiated, Radio-Frequency, Electromagnetic Field Immunity Test. International Electrotechnical Commission: Geneva, Switzerland, 2020. Available online: https://webstore.iec.ch/en/publication/59849 (accessed on 7 January 2026).
29. Pérez-Escribano, M.; Márquez-Segura, E. Parameters Characterization of Dielectric Materials Samples in Microwave and Millimeter-Wave Bands. *IEEE Trans. Microw. Theory Tech.* **2021**, *69*, 1723–1732. [CrossRef]